Hafnium Nitride with Thorium Phosphide Structure: Physical Properties and an Assessment of the Hf-N, Zr-N, and Ti-N Phase Diagrams at High Pressures and Temperatures

Peter Kroll*

Institut für Anorganische Chemie, Rheinisch-Westfälische Technische Hochschule Aachen (RWTH), Professor-Pirlet-Strasse 1, 52056 Aachen, Germany

(Received 20 November 2002; published 25 March 2003)

The physical properties of the new cubic phase of Hf_3N_4 as well as of isomorphic Zr_3N_4 and Ti_3N_4 are studied using first-principles calculations. Hf_3N_4, Zr_3N_4, and Ti_3N_4 are semiconductors with band gaps of 1.8, 1.1, and 0.6 eV, respectively. The band structure is characterized by the simultaneous presence of steep and extremely flat bands. The calculated shear modulus G indicates that the cubic Hf_3N_4 will be harder than the mononitride HfN. At ambient conditions, the cubic modifications of M_3N_4 (M = Hf, Zr, Ti) are metastable with respect to orthorhombic M_3N_4 phases, but the orthorhombic phases of Hf_3N_4 and Zr_3N_4 are stable with respect to the mononitrides and nitrogen.

DOI: 10.1103/PhysRevLett.90.125501 PACS numbers: 61.50.Ks, 64.70.Kb, 71.20.Nr, 81.30.Dz

The fourth-column transition metal mononitrides, TiN, ZrN, and HfN, are well known as hard materials used for cutting tools and wear protection. Because of their golden color, which is as bright as 24-carat gold, TiN and ZrN are also used as decorative coatings. They adopt the rock salt (NaCl) structure type, but may show significant variation in composition, both towards cation and anion rich. The refractory materials are conductors, having a residual electron per atom in the metal d bands and thus a significant density of states at the Fermi level. TiN, ZrN, and HfN are inherent superconductors with relatively high T_C's, 5.5, 10.7, and 8.8 K, respectively [1].

Most recently, Zerr *et al.* synthesized a novel hafnium nitride, Hf_3N_4, with a thorium phosphide (Th_3P_4) structure in the diamond-anvil cell at 18 GPa and 2800 K [2]. A semiconducting stoichiometric 3:4 nitride compound of Ti, Zr, or Hf was hitherto known for an orthorhombic Zr_3N_4 only [3,4]. The existence of the new cubic phase naturally leads to the question as to whether similar structures of Zr_3N_4 and Ti_3N_4 may also exist. Anticipating the results of this Letter, we find that indeed Zr_3N_4 and Ti_3N_4 will adopt the Th_3P_4 structure type at accessible pressures. The new modification with eight-coordinated cations may have very different physical properties that may lead to new applications. It is therefore, in general, useful to explore the physical properties of the new compounds. In particular, the recent synthesis of a cubic silicon nitride, γ-Si_3N_4, with spinel structure under quite similar conditions ($p = 15$ GPa, $T = 2000$ K) demonstrated the ability of theoretical calculations to predict a new phase and its properties [5]. By inspecting its shear modulus the hardness of γ-Si_3N_4 was predicted to be very high and third only to diamond and cubic boron nitride. Experimental studies confirmed this theoretical prediction later [6]. Meanwhile, γ-Si_3N_4 is produced in the 100 g scale by shock synthesis and used as an abrasive for final polishing [7].

More interest in nitrides of Hf and Zr stems from the fact that, in 1998, Yamanaka and co-workers discovered superconductivity ($T_C = 26$ K) in electron-doped β-HfNCl [8]. The mother compound β-HfNCl itself is a semiconductor with a large band gap $E_{gap} \approx 4$ eV. Similar effects have been discovered for other hafnium and zirconium nitride halides (MNX, M = Zr, Hf; X = Cl, Br, I) too.

In this Letter, we report detailed first-principles calculations of physical properties of Hf_3N_4, Zr_3N_4, and Ti_3N_4 in the Th_3P_4 structure. Moreover, we access the thermodynamical stability of the compounds within the respective metal-nitrogen phase diagram with respect to the mononitrides and nitrogen. We have used the VASP program to optimize structures and to calculate total energies and the electronic structures [9,10]. The ultrasoft pseudopotentials we used are based on the projector-augmented-wave method [11]. Both the local density approximation (LDA) [12] and the generalized-gradient approximation (GGA) [13] are employed: the LDA for structure, electronic, and elastic properties and frequencies, the GGA for calculating structure, energy, and enthalpy differences and, especially, transition pressures. All results rely on well-converged structures with respect to cutoff energy (500 eV) and **k**-point sampling. Tests using "hard" pseudopotentials showed no significant differences. The method is known for its accuracy, and recent successful examples are found within prediction and validation of SiO_2 phases [14], γ-Si_3N_4 [5], and of the P_3N_5 phase diagram [15]. The tight-binding linear combination of muffin tin orbitals (TB-LMTO) method was used to analyze the electronic structure in more detail [16].

The high-pressure phase of hafnium nitride Hf_3N_4 adopts the Th_3P_4 structure. Its space group symmetry is $I\bar{4}3d$ (220); Hf atoms are in 12a and N atoms are in 16c. Hence, the crystallographic structure has two free parameters only: the lattice constant a and the positional

 © 2003 The American Physical Society

parameter x of the N position. Despite its simplicity in terms of free parameters, however, it is difficult to visualize. Elaborate descriptions to apprehend the structure are given elsewhere [17]. The local environments, nevertheless, are much more simple (see Fig. 1): Hf is coordinated by 8 N atoms forming $\{\mathbf{Hf}\}N_8$ bisdisphenoids. The eight surrounding N atoms build two tetrahedra intergrown into each other, one elongated towards the axial positions of the bisdisphenoids, the other squashed towards the equatorial plane. N is coordinated by six Hf forming $\{\mathbf{Hf}\}N_6$ metaprisms, an environment between octahedral and trigonal prismatic. The metaprisms share common faces and are stacked parallel to the body diagonals of the cubic cell ($\langle 111\rangle$ direction) constituting a 3D packing of nonintersecting rods (Fig. 1).

All Hf-N bonds in the structure are equal in length, if the positional parameter $x = \frac{1}{12} = 0.0833$. For Hf_3N_4 we calculated $a = 6.5890$ Å (6.7149 Å) and $x = 0.0706$ ($x = 0.0671$) within the LDA (GGA values in parentheses). This agrees nicely with the experimental results of Zerr *et al.,* who report $a = 6.701$ Å [2]. The deviation of x from $\frac{1}{12}$ results in two different bond lengths Hf-N of 2.19 and 2.37 Å (2.21 and 2.45 Å). The equatorial bond lengths of the $\{\mathbf{Hf}\}N_8$ bisdisphenoids are the shorter Hf-N bonds, the axial bond lengths the longer ones. Within the $\{\mathbf{N}\}Hf_6$ metaprisms the different Hf-N bond lengths cause a shift of the N atom towards the basal plane. For comparison, we calculated the Hf-N bond length in the mononitrides HfN to 2.23 Å (2.27 Å). Results of Th_3P_4 structures of Zr_3N_4 and Ti_3N_4 are given in Table I.

The band structure of Hf_3N_4 is presented in Fig. 2 together with the corresponding density of states (DOS). Hf_3N_4 is a semiconductor with an indirect band gap E_{gap} of 1.8 eV (1.1 eV in GGA). The band gap is smaller for Zr_3N_4 and Ti_3N_4; see Table I. The band structure, nevertheless, is qualitatively the same for all compounds. The top of the valence band is about a quarter on the way between Γ and H; the bottom of the conduction band is at Γ. Since density functional theory calculations typically underestimate E_{gap} significantly (in most cases just 50%–80% of the experimentally observed E_{gap}), the true band gap should be in a region interesting for optical applications. Analyzing the *crystal orbital Hamilton population* (COHP [18]) within the LMTO method shows that all states up to the Fermi level contribute to Hf-N bonding; see Fig. 2. States at the lower edge of the conduction band are Hf-N antibonding, but Hf-Hf bonding. By integrating the COHP values up to the Fermi level we find −2.2 eV for the shorter Hf-N bonds and −1.6 eV for the longer Hf-N bonds; the more negative value indicates a stronger bond. In comparison, the value we obtain for the Hf-N bond in HfN is −2.1 eV; the lower bonding is due to Hf-N antibonding states just below the Fermi level. The shorter Hf-N bond in Hf_3N_4 thus appears optimized in both bond length and bond strength.

TABLE I. Structural data of Hf_3N_4, Zr_3N_4, and Ti_3N_4, with Th_3P_4 structure.

	Hf_3N_4		Zr_3N_4		Ti_3N_4	
	LDA	GGA	LDA	GGA	LDA	GGA
a (Å)	6.5890	6.7149	6.6943	6.8116	6.1859	6.3661
x	0.0706	0.0671	0.0728	0.0687	0.0720	0.0580
V_0 (Å^3/f.u.)	71.51	75.69	75.00	79.01	59.18	64.50
B_0 (GPa)	283	215	265	195	270	235
E_{gap} (eV)	1.8	1.1	1.1	0.7	0.6	0.45

Interestingly, the DOS of Hf_3N_4 shows several pronounced peaks, e.g., −1.4 and −1.8 eV below the top of the valence band, which correspond to extremely flat bands in the band structure. These bands belong to delocalized Hf_d-N_p bonding states, but obviously without significant dispersion. Steep bands are also observed (follow the Γ topmost band towards H or P, and its unfilled counterpart). The simultaneous presence of steep and extremely flat band portions around the Fermi level has been recognized as a "fingerprint" for a potentially superconducting compound [19]. It is therefore quite possible that superconductivity will be present after doping the material, either by substitution of elements or by filling the interstices at the $12b$ position of the Th_3P_4 structure type.

For the elastic constants of Hf_3N_4 we found $c_{11} = 521$ GPa, $c_{12} = 174$ GPa, and $c_{44} = 163$ GPa (LDA results). Since $\frac{1}{2}(c_{11} - c_{12}) \approx c_{44}$ holds, Hf_3N_4 behaves

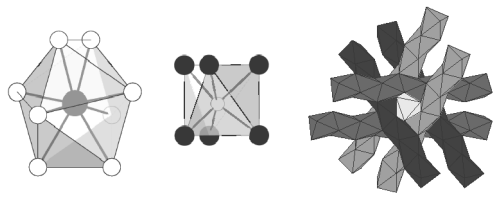

FIG. 1. Coordination polyhedra of atoms in Hf_3N_4: the $\{\mathbf{Hf}\}N_8$ bisdisphenoid (left) and the $\{\mathbf{N}\}Hf_6$ metaprism (middle). On the right the 3D packing of nonintersecting rods in the Th_3P_4 structure type is shown (projection down [111]).

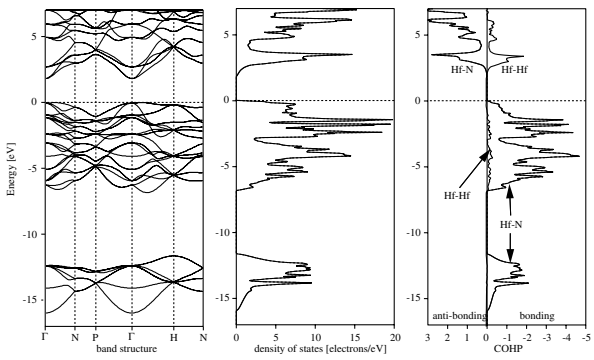

FIG. 2. Band structure, corresponding density of states (DOS), and COHP of Hf_3N_4 calculated using the LDA within the TB-LMTO method. The top of the valence band is set to zero energy.

almost like a completely isotropic material. The numerical values are further used to estimate bulk modulus B and shear modulus G according to the methods of Voigt and Reuss [20]: Both approaches give identical results, $B = 290$ GPa and $G = 167$ GPa. The bulk modulus B obtained via standard volume compression is 283 GPa (215 GPa within the GGA). Taking B and G we estimate Young's modulus, $E = 420$ GPa and Poisson ratio, $\nu = 0.26$.

For the mononitride HfN we calculated $c_{11} = 602$ GPa, $c_{12} = 169$ GPa, and $c_{44} = 69$ GPa. Thus, $B = 313$ GPa (310 GPa calculated via compression, GGA: 270 GPa). The shear modulus G comes out to 110 GPa by averaging the two rather different values of G obtained by the methods of Voigt and Reuss. Young's modulus $E = 295$ GPa and Poisson ratio $\nu = 0.34$ are comparable with experimental values of $E = 380$ GPa and $\nu = 0.35$ [21]. Therefore, although the bulk modulus of Hf_3N_4 is smaller than that of HfN, its Young's modulus as well as its shear modulus is larger. Since the latter is the best indicator for hardness, we expect Hf_3N_4 to be somewhat harder than HfN (Vickers hardness of 14 GPa [22]).

We computed the zone-center vibrational spectra of Hf_3N_4, Zr_3N_4, and Ti_3N_4 to support phase characterization by the micro-Raman technique. The Th_3P_4 structure of Hf_3N_4 has point group T_d and its primitive unit cell contains 14 atoms. The group theoretical analysis of 39 ($=3 \times 14$-3) optical modes yields the decomposition of the reducible representation according to $\Gamma^{\text{opt}} = A_1 + 2A_2 + 3E + 5T_1 + 5T_2$. A_1, E, and T_2 modes are Raman active, T_2 modes are also IR active. The results of zone-center phonon modes obtained by diagonalizing the dynamical matrix generated via finite-difference methods are listed in Table II.

Zerr *et al.* report only two modes of Hf_3N_4 with high intensity at 420 and 730 cm^{-1} that we can identify as of E and T_2 symmetry. Noteworthy, the A_1 mode at 362 cm^{-1} corresponds to an asymmetrical stretching vibration (hence, movement) of N atoms within the rods.

To access the thermodynamical stability of Hf_3N_4 and to explore the phase diagrams of Hf-N, Zr-N, and Ti-N, we investigated further possible structural modifications of 3:4 compounds. Most surprisingly, two other—albeit still hypothetical—modifications of Hf_3N_4 turned out to be lower in energy at zero pressure than the Th_3P_4 structure type of Hf_3N_4: a spinel modification ($Fd\bar{3}m$, $a = 9.065$ Å; by 0.4 eV/Hf_3N_4) as well as a Zr_3N_4-type modification ($Pna2_1$, $a = 9.83$ Å, $b = 10.27$ Å, $c = 3.245$ Å; by 0.5 eV/Hf_3N_4). We also considered a defect NaCl-type structure, in which only 75% of the cation sites are occupied. This $Hf_{0.75}N$, however, comes out to be substantially higher in energy by more than 2 eV/Hf_3N_4. An assessment of configurational (mixing) entropy for this defective structure, for which we calculate $S = 18.7$ JK^{-1} per Hf_3N_4, shows that entropic effects will not overcome this large energy difference even at 2000 K. For each structure type we calculated complete energy-volume (E-V) diagrams for Hf_3N_4, Zr_3N_4, and Ti_3N_4 including full structural optimization under the constraint of constant volume. They are shown in Fig. 3 on the left side.

We then calculate enthalpy $H = E + pV$ and pressure p; the latter can be extracted from the E-V graph by numerical differentiation of a spline fit to the data. The resulting enthalpy-pressure (ΔH-p) diagrams of Hf_3N_4, Zr_3N_4, and Ti_3N_4 with reference to the lowest energy structure (Zr_3N_4 type) are given in Fig. 3 on the right side. Both E-V and ΔH-p diagrams show that in every system the orthorhombic Zr_3N_4-type structure constitutes the lowest energy modification, while the cubic Th_3P_4 type will be adopted for small volumes, hence, at high pressures. The synthesized cubic Hf_3N_4, therefore, is a metastable compound with significant energy difference (0.5 eV/f.u.) to the not-yet-synthesized lowest energy Zr_3N_4-type modification of Hf_3N_4. In every system, the spinel modification comes close to the Zr_3N_4 type in energy at zero pressure, but evidently has an unfavorable

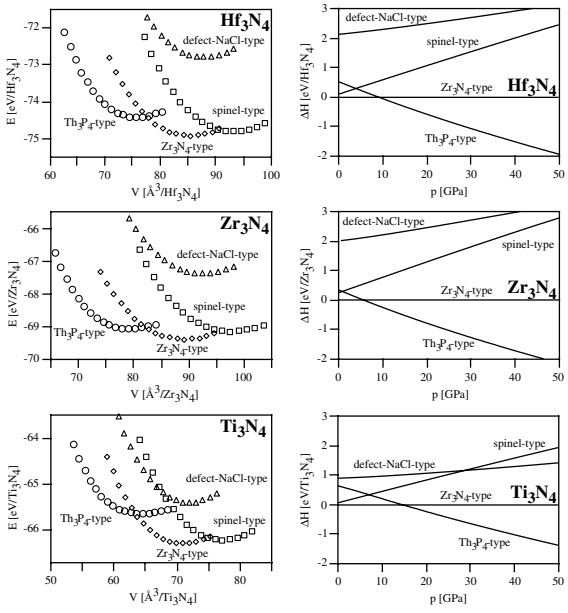

FIG. 3. Energy-volume (E-V) diagrams (left) and enthalpy-pressure (ΔH-p) diagrams (right, relative to the Zr_3N_4 type) of different structural modifications of Hf_3N_4 (top panels), Zr_3N_4 (middle panels), and Ti_3N_4 (bottom panels). Circles, diamonds, squares, and triangles correspond to the structure types of Th_3P_4, Zr_3N_4, spinel, and defective NaCl, respectively.

TABLE II. Raman-active phonon modes of Hf_3N_4, Zr_3N_4, and Ti_3N_4 in Th_3P_4 structure (in cm^{-1}). The T_2 modes are also IR active.

	E	E	T_2	T_2	T_2	A_1	T_2	E	T_2
Hf_3N_4	695	640	537	432	368	362	229	127	111
Zr_3N_4	670	609	506	423	368	336	282	165	142
Ti_3N_4	738	637	534	470	452	345	297	175	162

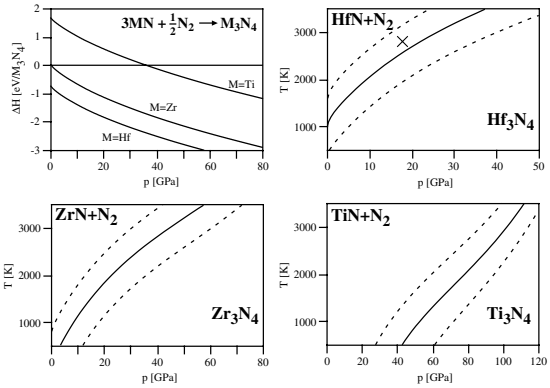

FIG. 4. Top left: ΔH of the reactions $3MN + \frac{1}{2}N_2 \rightarrow M_3N_4$ (M = Hf, Zr, Ti) at zero temperature as a function of pressure. Top right and bottom: p, T diagrams of the reactions $3MN + \frac{1}{2}N_2 \rightarrow M_3N_4$ (M = Hf, Zr, Ti). The solid lines correspond to phase equilibria ($\Delta G = 0$); the dashed lines correspond to $\Delta G = +0.5$ and $\Delta G = -0.5$. The cross in the Hf-N phase diagram indicates the experimental conditions of Zerr *et al.* [2].

compression behavior, as has the defect-NaCl structure type too. We calculate the transition pressures of the Zr_3N_4-type $\rightarrow$ Th_3P_4-type transition to 9, 6, and 16 GPa for Hf_3N_4, Zr_3N_4, and Ti_3N_4, respectively.

The enthalpy difference ΔH is a good measure to compare the relative stability of solid state structures under pressure, because their entropy differences that contribute to the free enthalpy ΔG are typically small. The situation, however, is inherently more complicated if one side of the reaction comprises a gaseous product, such as in the nitridation reaction $3MN + \frac{1}{2}N_2 \rightarrow M_3N_4$ (M = Hf, Zr, Ti). In such a case, the inclusion of entropic effects of the gas is mandatory. To access the thermodynamical stability of Hf_3N_4, Zr_3N_4, Ti_3N_4 with respect to the mononitride and nitrogen gas as a function of pressure, therefore, we need to augment the calculated enthalpy with the free enthalpy ΔG of nitrogen, taken as a function of temperature and pressure. This quantity incorporates, at least to first order, all temperature effects of the reaction. The thermochemical data of nitrogen are taken from standard reference data [23]. The resulting p, T diagrams of the nitridation of HfN, ZrN, and TiN are shown in Fig. 4. For reference, we included the ΔH-p diagram for each reaction. The diagram shows that within the outlined approximation we are able to reproduce the experimental conditions of Zerr *et al.* [2]. Furthermore, we predict that by using a similar experimental approach (T = 2800 K), a Th_3P_4-type Zr_3N_4 becomes accessible at 45 GPa, a Ti_3N_4 requires about 100 GPa.

In summary, we characterized structural, electronic, elastical, vibrational, and thermodynamical properties of the new cubic Hf_3N_4 compound and isotopic Zr_3N_4 and Ti_3N_4 using first-principles calculations. The band structure shows fingerprints necessary for the appearance of superconductivity, which may occur after appropriate doping. The thermodynamical assessment establishes that cubic modifications of Zr_3N_4 and Ti_3N_4 also exist, but are metastable in each system. Thus, the energetically more stable orthorhombic modifications can be obtained if a decomposition into mononitrides and nitrogen is avoided. Since the orthorhombic Zr_3N_4 can be synthesized via ammonolysis of $ZrCl_4$ [4], we propose this phase to use as a precursor for the synthesis of cubic Zr_3N_4 at about 6 GPa. Nevertheless, the nitridation of the mononitrides at 2800 K should yield cubic phases of Zr_3N_4 and Ti_3N_4 at 45 and 100 GPa, respectively.

The author is grateful to R. Dronskowski, A. Zerr, J. Golzewski, and J.-W. Seok for fruitful discussions. This work was supported by the DFG (Kr1805/5-1).

*Electronic address: peter.kroll@ac.rwth-aachen.de

[1] H. O. Pierson, *Handbook of Refractory Carbides and Nitrides: Properties, Characteristics, and Applications* (Noyes Publications, Westwood, NJ, 1996).
[2] A. Zerr, G. Miehe, and R. Riedel, Nature Materials **2**, 185 (2003).
[3] R. Juza *et al.*, Z. Anorg. Allg. Chem. **332**, 1 (1964).
[4] M. Lerch, E. Füglein, and J. Wrba, Z. Anorg. Allg. Chem. **622**, 367 (1996).
[5] A. Zerr *et al.*, Nature (London) **400**, 340 (1999).
[6] A. Zerr *et al.*, J. Am. Ceram. Soc. **85**, 86 (2002).
[7] T. Sekine, J. Am. Ceram. Soc. **85**, 113 (2002).
[8] S. Yamanaka, K. Hotehama, and H. Kawaji, Nature (London) **392**, 580 (1998).
[9] G. Kresse and J. Hafner, Phys. Rev. B **47**, 558 (1993); **49**, 14 251 (1994).
[10] G. Kresse and J. Furthmüller, Phys. Rev. B **54**, 11 169 (1996).
[11] G. Kresse and D. Joubert, Phys. Rev. B **59**, 1758 (1999).
[12] J. P. Perdew and A. Zunger, Phys. Rev. B **23**, 5048 (1981).
[13] J. P. Perdew, in *Electronic Structure of Solids '91*, edited by P. Ziesche and H. Eschrig (Akademie Verlag, Berlin, 1991), p. 11.
[14] D. M. Teter *et al.*, Phys. Rev. Lett. **80**, 2145 (1998).
[15] P. Kroll and W. Schnick, Chem. Eur. J. **8**, 3530 (2002).
[16] O. K. Andersen *et al.*, The Stuttgart TB-LMTO-ASA Program version 47, MPI für Festkörperforschung, Stuttgart, Germany, 1996.
[17] M. O'Keeffe and B. G. Hyde, *Crystal Structures. I. Patterns and Symmetry* (Mineralogical Society of America, Washington, D.C., 1996), p. 237f.
[18] R. Dronskowski and P. E. Blöchl, J. Phys. Chem. **97**, 8617 (1993).
[19] A. Simon, Angew. Chem., Int. Ed. Engl. **36**, 1788 (1997).
[20] G. Grimval, *Thermophysical Properties of Materials* (North-Holland, Amsterdam, 1986).
[21] A. J. Perry, Thin Solid Films **193**, 463 (1990).
[22] M. Desmaison-Brut *et al.*, J. Eur. Ceram. Soc. **13**, 379 (1994).
[23] M. W. Chase, Jr., *NIST-JANAF Thermochemical Tables*, Journal of Physical and Chemical Reference Data, Monograph 9 (AIP, Washington, D.C., 1998), 4th ed.